

Article

Research on the Mixing Mechanism and Parameter Optimization of Liquid Nitrogen Foam Generator

Yulin Liu ¹, Dongming Wang ¹, Min Xie ^{2,*} , Huanhuan Xu ^{3,*} and Xiaohan Ren ^{1,*} ¹ Institute of Thermal Science and Technology, Shandong University, Jinan 250061, China² Harbin Electric Science and Technology Co., Ltd., Harbin 150028, China³ National Engineering Laboratory for Reducing Emissions from Coal Combustion, School of Energy and Power Engineering, Shandong University, Jinan 250061, China

* Correspondence: alice.m.xie@icloud.com (M.X.); xuhuanhuan@sdu.edu.cn (H.X.); renxh@sdu.edu.cn (X.R.)

Abstract: Nitrogen foam is expected to be an effective method to extinguish large-scale fires and suppress explosions. The key to its foaming process is that gas nitrogen (N₂) and a foam solution are mixed uniformly in a foam generator. Moreover, liquid nitrogen (LN₂) has been proposed as a source of gas nitrogen to generate nitrogen foam in previous experimental works. In this paper, the flow and heat transfer characteristics between liquid nitrogen and the foam solution are explored by numerical methods, which are then utilized to optimize the parameters of the foam generator. It is found that the flow pattern of the foam generator with a cone spoiler is a stratified flow by establishing the mixture and Lee's evaporation-condensation model in ANSYS Fluent. Moreover, the spoiler in the foam generator plays a crucial role in breaking LN₂ into droplets and increasing the contact area between phases, and a distance of 10 mm from the inlets to the spoiler is recommended. From previous results, an unreasonable flow rate ratio of LN₂ to a foam solution may lead to icing or a low volume fraction of nitrogen, thus a flow rate ratio of 1:50 is determined in the foam generator. As for the shape of the spoiler, the spiral spoiler shows the best foaming performance compared to cone and semisphere spoilers, due to its fluid rotation instead of translation, which effectively increases the N₂ volume fraction of foam from 0.616 to 0.717. Therefore, the mixing characteristics of the foam generator in this work lays a foundation for devising a practical nitrogen foam generator.

Keywords: nitrogen foam; computer fluid dynamics (CFD); rapid phase transition (RPT); multiphase flow



Citation: Liu, Y.; Wang, D.; Xie, M.; Xu, H.; Ren, X. Research on the Mixing Mechanism and Parameter Optimization of Liquid Nitrogen Foam Generator. *Energies* **2022**, *15*, 8714. <https://doi.org/10.3390/en15228714>

Academic Editor: Abu-Siada Ahmed

Received: 12 October 2022

Accepted: 14 November 2022

Published: 20 November 2022

Publisher's Note: MDPI stays neutral with regard to jurisdictional claims in published maps and institutional affiliations.



Copyright: © 2022 by the authors. Licensee MDPI, Basel, Switzerland. This article is an open access article distributed under the terms and conditions of the Creative Commons Attribution (CC BY) license (<https://creativecommons.org/licenses/by/4.0/>).

1. Introduction

With the boost of oil reserves, oil tanks tend to be large and clustered, increasing the possibility of fire [1]. The oil and its byproducts in the tanks are easy to burn and explode, and then produce a large number of hazardous substances, which bring expensive losses to safety and property [2]. Fire extinguishing technologies are further refined to deal with fires caused by oil. The frequently used fire extinguishing systems usually consist of water systems and compressed air foam systems (CAFS). Water systems rely on thermal shielding to decrease temperatures, which only works on small-scale fires [3], and show limited effectiveness in fuel pool fires and enclosure fires [4]. A CAFS is an effective approach to large-scale fires, and it uses a compressed air and foam solution to generate compressed air foam. The foam solution is usually composed of 97% water and 3% aqueous film-forming foam (AFFF) to reduce the surface tension of water and then mix foam solution with compressed air [5]. The compressed air foam is light and porous, and it can expand the volume of air in the form of foam to increase the area covering the fire, but the use of a large compressor limits its application. In addition, compressed air foam is not as effective as nitrogen foam in inhibiting combustion and explosion, because of the inert properties of N₂ [6]. Compared with other fire-extinguishing gas, like carbon dioxide (CO₂), the gas nitrogen is easier to be separated from air, leading to a lower cost [7]. Thus, it is important to find a reasonable way to utilize nitrogen foam due to its outstanding advantages.

The principles of extinguishing fire with nitrogen foam are shown as follows [8]: (1) cooling effect: when the nitrogen foam enters the fire, the water in the foam will absorb heat and evaporate rapidly, which can reduce the temperature of the fire; (2) suffocation effect: after being injected into a high-temperature fire, the nitrogen initially encapsulated in the foam will be released [9] to dilute the oxygen concentration and keep the fire area inert [10]. Then, the foam will drain and release gas nitrogen over a long time, which is conducive to preventing secondary combustion; and (3) isolation effect: when the nitrogen foam covers the fire, it will absorb a large amount of radiant heat and prevent heat from transferring to another combustible substance, which also allows the combustion area to be controlled.

Nowadays, nitrogen foam replaces compressed air foam in some closed areas, such as mine fires and sand washing [11,12]. Zhou et al. [13] utilized three-phase foam, including coal fly ash (or slurry), N_2 , and water, to prevent or mitigate the Baijigou coal mine fire. The three-phase nitrogen foam can expand 30 times the volume of nitrogen, which effectively isolated and controlled the oxygen (O_2) concentration below 5%. Lu et al. [14] introduced a cavitation jet device, which improved the stability of foam to quell large-scale coal fires in open-pit mines. The results showed that nitrogen foam could decrease the temperature of the fire by 6–7 times more than that of water and reduce the concentration of carbon monoxide (CO) from 9.43% to 0.092%. The proofs are that N_2 has a remarkable effect on fire extinguishing, while there are still some barriers to the storage of gas nitrogen. Thus, liquid nitrogen has been proposed as an alternative to gas nitrogen, owing to its high-density ratio (liquid nitrogen to gas nitrogen is about 700:1 [15]), easy storage, and low temperature [16]. When LN_2 contacts with foam solution, it will absorb a large amount of heat from the foam solution and then evaporate into gas nitrogen instantly [17]. Then the nitrogen mixes with the foam solution to form nitrogen foam.

The foam solution is composed of 97% water and 3% AFFF solution, hence some attention has been paid to LN_2 injected into water. Clarke et al. [17] conducted a visual experiment where LN_2 was injected into a pressure vessel containing water. The contributions of pressurization from the mass transfer, latent heat transfer, and sensible heat transfer were solved, and warm water was illustrated as the latent heat source of LN_2 . A four-stage evolution of the jet structure was revealed, including gaseous preinjection, liquid injection, impact with the opposing wall, and buoyancy-driven break-up stage. The thin vapor film wrapped in the LN_2 could be noticed when the LN_2 was injected. One of the lessons was that the jet structure had a great impact on the interface between LN_2 and warm fluid. Rupak et al. [18] investigated the interfacial behavior of the LN_2 boiling over the water surface, and the ice formation caused by a low temperature changed the interfacial activities. Rayleigh-Taylor instability was set as a criterion to distinguish no bubbling, moderate bubbling, or vigorous bubbling, on basis of the release of N_2 from the entrapped liquid layers.

The RPT process of liquified natural gas (LNG) is useful, attributed to its similarity to LN_2 [19]. Saleem et al. [20] set up a comprehensive CFD model of a full-scale LNG tank, which aimed to avoid heat leakage from the surroundings into an LNG storage tank, in case of boil-off-gas (BOG). The volume of fluid (VOF) model was used to observe the vapor-liquid interface, and Lee's evaporation-condensation model was employed to explain the phase transition concerning the effect of static pressure. Heat ingress magnitude, internal flow dynamics, and convective heat transfer were further investigated to account for the boiling phenomenon. The critical wall superheat of the LNG transition from surface evaporation to nucleate boiling was estimated as 2.5–2.8 K.

The characteristics of flow and heat transfer have a significant impact on the foaming process, in which spoilers are widely used to enhance the turbulence intensity [10]. Zhou et al. [21] studied the flow characteristics of liquid nitrogen foam in a horizontal foam generator in experimental and numerical methods. A mixture model and Lee's evaporation-condensation model were established by ANSYS Fluent. The conclusion was that RPT enhanced the heat and mass transfer, and the conical spoiler facilitates the fluid turbulence.

Six flow patterns were concluded according to the flow and heat transfer characteristics, which were instrumental in utilizing an LN₂ foam generator. Lu et al. [22] investigated the pressure gradient and the performance of a spiral-mesh foam generator. The research showed that its pressure gradient increased with the foam concentration in water. The uniform foam was formed in the middle section of the pipe due to few pressure changes, although the pressure gradient gap at both ends of the foam generator was large. When the pressure gradient exceeded the minimum pressure gradient, the foam production quantity would increase sharply. The optimal range of the flow rate of air was set at 50–60 m³·h⁻¹ when the foam concentration in water was 0.6%.

Compressed air foam and nitrogen foam are non-Newtonian fluids with shear-thinning properties and two-phase homogeneous fluids [23]. Although their foaming processes are complex, they are valuable for fire extinguishing. Some experimental conclusions have been drawn from previous work that the foam generator, assisted by a spoiler, will intensify the mass and heat transfer between liquid nitrogen and the foam solution to improve its foaming performance [21]. However, it is difficult to do a quantitative analysis of the RPT process in experiments. In this work, we study the flow and heat transfer characteristics of a foam generator with a cone spoiler. It is found that the spoiler plays an important role in enhancing the turbulent intensity of the foaming process. When the foam generator is equipped with a cone spoiler, its flow pattern is a stratified flow. Then, some factors affecting the performance of the foam generator, such as the distance between the inlets and spoiler, the flow rate of liquid nitrogen, and the shape of the spoiler are investigated to find out the best working condition. According to the results, the foam generator with a distance between inlets and spoiler of 10 mm, a flow rate of liquid nitrogen to foam solution of 1:50, and a foam generator with a spiral spoiler performs best. Moreover, the RPT process of cryogenic liquid not only includes the evaporation of liquid nitrogen but also covers LNG storage [24], the cryogenic propellant for fuel [25], which helps to gain a deeper insight into the theoretical foundation for heat and mass transfer between phases.

2. Models

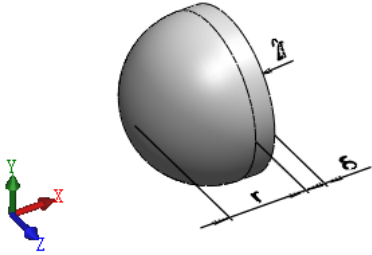
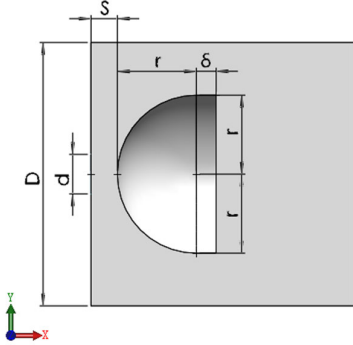
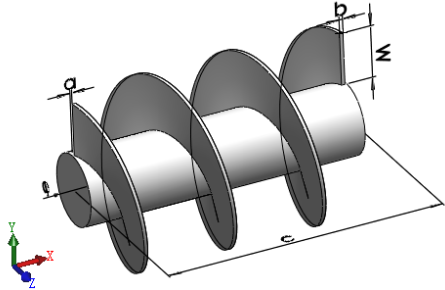
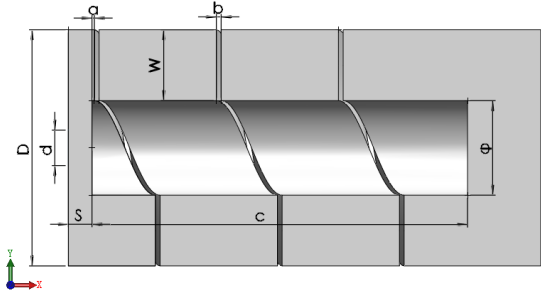
2.1. Geometry Models

In this work, the foam generator is the fluid domain as shown in Table 1. The foam generator is with a diameter (D) of 100 mm and a length (L) of 1000 mm. An inner circular LN₂ inlet and an annular foam solution inlet constitute the diameter (D) of the foam generator. The diameter (d) of the LN₂ inlet is 15 mm, and the inner diameter and outer diameter of the foam solution inlet (annular shape) are 15 mm and 100 mm, respectively. A spoiler is put on the central axis of the foam generator with a distance (S) between the inlets and the spoiler, and the detailed parameters are shown in Table 1. The foam generator without a spoiler is as a control, and the foam generator with a cone spoiler is used to solve the optimal distance and the LN₂ flow rate. Then the foam generators with other spoilers are simulated using solved parameters to determine the best shape for spoilers. The thermal properties of the fluid are listed in Table 2, including nitrogen, foam solution, and liquid nitrogen.

Table 1. The geometric dimensions of the foam generator and spoilers.

Item	Geometry	Profile of the Computational Fluid Domain *	Parameters
Foam generator		$D = 100 \text{ mm}$ $d = 15 \text{ mm}$ $L = 1000 \text{ mm}$ S is the distance between inlets and spoiler	
(a) Cone spoiler			$l = 60 \text{ mm}$ $\delta = 7.5 \text{ mm}$

Table 1. Cont.

Item	Geometry	Profile of the Computational Fluid Domain *	Parameters
(b) Semisphere spoiler			$r = 30 \text{ mm}$ $\delta = 7.5 \text{ mm}$
(c) Spiral spoiler			$\phi = 40 \text{ mm}$ $a = 1 \text{ mm}$ $b = 2 \text{ mm}$ $c = 159 \text{ mm}$ $W = 30 \text{ mm}$

* The whole length of the computational fluid domain is L , and only the main parts are given in the table.

Table 2. The thermal properties of materials *.

Item	Density	Specific Heat	Thermal Conductivity	Standard State Enthalpy
	kg·m ⁻³	J·kg ⁻¹ ·K ⁻¹	W·m ⁻¹ ·K ⁻¹	J·kg ⁻¹ ·mol ⁻¹
N ₂	1.14	Piecewise-polynomial	0.0242	2792.8
Foam solution	998.20	4182.0	0.6000	–
LN ₂	806.08	2014.5	0.1458	–

* Data from the material database of ANSYS Fluent.

2.2. Mathematical Models

The LN₂ injected into water will undergo an RPT process and then evaporate into nitrogen. Owing to the low surface tension of the foam solution, nitrogen and water will form a homogeneous nitrogen foam. The complexity of the RPT brings great challenges for experiments to analyze quantitatively. Assisted with the simulation, the mechanism of the RPT, and the foaming process can be settled. The renormalization group (RNG) k - ε turbulence model is fit for the simulation, improving the accuracy of the standard k - ε model for swirling flows caused by the spoiler [26]. The mixture model is determined because the nitrogen foam is a multiphase mixture and is assumed to be a homogeneous mixture. The nitrogen is taken as the primary phase, and the foam solution and LN₂ are the secondary phases. Liquid nitrogen evaporates into nitrogen, hence Lee's evaporation-condensation model is indispensable [10]. All the mathematical models are built by ANSYS Fluent, a commercial CFD software using the finite volume method.

2.2.1. Turbulence Models

The RNG k - ε model has a similar form to the standard k - ε model, where k is the turbulent kinetic energy and ε is the dissipation rate [27], as follows:

k -equation:

$$\frac{\partial}{\partial t}(\rho k) + \frac{\partial}{\partial x_i}(\rho k u_i) = \frac{\partial}{\partial x_j} \left[\sigma_k \mu_{eff} \frac{\partial k}{\partial x_j} \right] + G_k + G_b - \rho \varepsilon - Y_M \quad (1)$$

ε -equation:

$$\frac{\partial}{\partial t}(\rho \varepsilon) + \frac{\partial}{\partial x_i}(\rho \varepsilon u_i) = \frac{\partial}{\partial x_j} \left[\sigma_\varepsilon \mu_{eff} \frac{\partial \varepsilon}{\partial x_j} \right] + C_{1\varepsilon} \frac{\varepsilon}{k} (G_k + G_{3\varepsilon} G_b) - C_{2\varepsilon} \rho \frac{\varepsilon^2}{k} - R_\varepsilon \quad (2)$$

$$\mu_{eff} = \mu + \mu_t \quad (3)$$

$$\mu_t = \rho C_\mu \frac{k^2}{\varepsilon} \quad (4)$$

where ρ is the density of the fluid, u_i is the mean velocity component in the x_i axis, μ_{eff} is the effective turbulent viscosity, μ is the dynamic viscosity, μ_t is the turbulent viscosity, and C_μ is a constant. The G_k represents the generation of turbulence kinetic energy due to the mean velocity gradients, G_b is the generation of turbulence kinetic energy due to buoyancy, Y_M represents the contribution of the fluctuating dilatation in compressible turbulence to the overall dissipation rate, the quantities σ_k and σ_ε are the inverse effective Prandtl numbers for k and ε , and $C_{1\varepsilon}$, $C_{2\varepsilon}$, $C_{3\varepsilon}$ are constants.

2.2.2. Mixture Multiphase Models

The mathematical model proposed in this study is a simplified two-fluid model, where liquid nitrogen and foam solution are thought to be interpenetrating continua. The flow of nitrogen foam, as a mixture, is calculated according to continuity and a Navier-Stokes equation [28]. The formulas are shown below:

(1) Continuity equation

$$\frac{\partial \rho_m}{\partial t} + \nabla \cdot (\rho_m \vec{v}_m) = 0 \quad (5)$$

$$\rho_m = \sum_{k=1}^n \alpha_k \rho_k \quad (6)$$

$$\vec{v}_m = \frac{\sum_{k=1}^n \alpha_k \rho_k \vec{v}_k}{\rho_m} \quad (7)$$

where ρ_m is the mixture density, t is time, \vec{v}_m is the velocity of the mass center, α_k is the volume fraction of phase k , and n is the number of phases.

(2) Momentum equation

$$\frac{\partial}{\partial t} (\rho_m \vec{v}_m) + \nabla \cdot (\rho_m \vec{v}_m \vec{v}_m) = -\nabla p + \nabla \cdot \left[\mu_m \left(\nabla \vec{v}_m + \nabla \vec{v}_m^T \right) \right] + \rho_m \vec{g} - \nabla \cdot \left(\sum_{k=1}^n \alpha_k \rho_k \vec{v}_{dr,k} \vec{v}_{dr,k} \right) + M_m \quad (8)$$

$$\mu_m = \sum_{k=1}^n \alpha_k \mu_k \quad (9)$$

$$\vec{v}_{dr,k} = \vec{v}_k - \vec{v}_m \quad (10)$$

$$M_m = \sum_{k=1}^n M_k \quad (11)$$

where p is the pressure, μ_m is the viscosity of the mixture, $\vec{v}_{dr,k}$ is the drift velocity of secondary phase k , M_m is the influence of the surface tension force on the mixture, and M_k is the influence of the surface tension force on the secondary phase k .

(3) Energy equation

$$\frac{\partial}{\partial t} \sum_k (\alpha_k \rho_k E_k) + \nabla \cdot \sum_k (\alpha_k \vec{v}_k (\rho_k E_k + p)) = \nabla \cdot \left(k_{eff} \nabla T - \sum_k \sum_j h_{j,k} \vec{J}_{j,k} + (\vec{\tau}_{eff} \cdot \mathbf{v}) \right) + S_h \quad (12)$$

where $h_{j,k}$ is the enthalpy of species j in phase k , $\vec{J}_{j,k}$ is the diffusive flux of species j in phase k , T is the equilibrium temperature, k_{eff} is the effective conductivity calculated as $(\sum \alpha_k (k_k + k_t))$, k_k is the conductivity of phase k , and k_t is the turbulent thermal conductivity defined according to the turbulence model. The first three terms on the right-hand side of Equation (12) represent energy transfer due to conduction, species diffusion, and viscous dissipation, respectively. The source term S_h can be obtained in Equation (20) by multiplying the rate of mass transfer in Equation (17) and the latent heat.

For a compressible phase, E_k in Equation (12) can be expressed as:

$$E_k = h_k - \frac{p}{\rho_k} + \frac{v_k^2}{2} \quad (13)$$

E_k is the total energy of phase k , for an incompressible phase $E_k = h_k$, where h_k is the sensible enthalpy for phase k .

(4) Relative velocity and the drift velocity

The relative velocity is defined as the velocity of a secondary phase p , relative to the velocity of the primary phase q :

$$\vec{v}_{pq} = \vec{v}_p - \vec{v}_q \quad (14)$$

The mass fraction c_k for any phase k is defined as:

$$c_k = \frac{\alpha_k \rho_k}{\rho_m} \quad (15)$$

The drift velocity $\vec{v}_{dr.p}$ is calculated by the following expression:

$$\vec{v}_{dr.p} = \vec{v}_{pq} - \sum_{k=1}^n c_k \vec{v}_{kq} \quad (16)$$

where \vec{v}_{kq} is the velocity of phase k relative to phase q .

(5) Volume fraction equation of the secondary phase

From the continuous equation of phase p , the volume fraction equation for phase q can be obtained as:

$$\frac{\partial}{\partial t} (\alpha_p \rho_p) + \nabla \cdot (\alpha_p \rho_p \vec{v}_m) = -\nabla \cdot (\alpha_p \rho_p \vec{v}_{dr.p}) + \sum_{q=1}^n (\dot{m}_{qp} - \dot{m}_{pq}) \quad (17)$$

where \dot{m}_{qp} is the mass transfer from phase q to phase p , and \dot{m}_{pq} is in the same vein.

2.2.3. Evaporation-Condensation Models

When the temperature of LN₂ exceeds its saturation temperature, the RPT process takes place. The evaporation-condensation (Lee) model [29] is a mechanistic model with a physical basis, which can couple with mixture models. The liquid/vapor mass transfer (evaporation and condensation) is governed by the vapor transport equation:

$$\frac{\partial}{\partial t} (\alpha_v \rho_v) + \nabla \cdot (\alpha_v \rho_v \vec{v}_v) = \dot{m}_{lv} - \dot{m}_{vl} \quad (18)$$

where v is the vapor phase, α_v is vapor volume fraction, ρ_v is vapor density, \vec{v}_v is vapor phase velocity, and \dot{m}_{lv} and \dot{m}_{vl} are the rates of the mass transfer due to evaporation and condensation, respectively.

The model has defined positive mass transfer as being from the liquid to the vapor for evaporation-condensation problems. Based on the following temperature regimes, the mass transfer can be described as follows:

$$\begin{cases} \dot{m}_{lv} = coeff * \alpha_l \rho_l \frac{T_l - T_{sat}}{T_{sat}}, & \text{if } T_l > T_{sat} \text{ (evaporation)} \\ \dot{m}_{vl} = coeff * \alpha_v \rho_v \frac{T_{sat} - T_v}{T_{sat}}, & \text{if } T_v < T_{sat} \text{ (condensation)} \end{cases} \quad (19)$$

where the subscripts l and v represent that the phase states are liquid and gas. The *coeff* is a tunable coefficient and can be interpreted as a relaxation time. It is set to 0.1 in this paper, according to Refs. [13,20]. The variables α , ρ , and T are the phase volume fraction, density, and temperature, respectively. T_{sat} is the saturation temperature of LN₂, set as 77 K at atmospheric pressure.

The source term of S_h in the energy equation can be computed by:

$$\begin{cases} S_h = -\dot{m}_{lv} H_{lv}, & \text{if } T_l \geq T_{sat} \\ S_h = \dot{m}_{vl} H_{lv}, & \text{if } T_v < T_{sat} \end{cases} \quad (20)$$

where H_{lv} is the latent heat of the vaporization of liquid nitrogen.

2.3. Boundary Conditions

The LN₂ and the foam solution are incompressible liquids, therefore, the inner LN₂ inlet and annular foam solution inlet are set as velocity inlets, whose values in different cases are shown in Table 3. The temperatures of the LN₂ inlet and the foam solution inlet are 75 K and 293.15 K, respectively. The surface tension is set as 0.02 N·m⁻¹ between phases, in accordance with experiments [30]. The shells of the foam generator and the spoiler are set as walls with a temperature of 293.15 K (room temperature). The temperature was set as an ideal constant because the heat conduction, heat convection, and heat radiation of the wall are not the main heat transfer processes in the foam generator, but for the turbulent RPT process between the liquid nitrogen and the foam solution. The wall is a stationary wall with no slip and standard roughness to provide a reference for future engineering

applications. The pressure outlet is adopted with a pressure of 0 Pa, as the nitrogen foam flows into the atmosphere. In this work, the distance between inlets and spoiler, LN₂ flow rate, and spoiler shape are variables, and all working conditions are shown in Table 3.

Table 3. The working conditions for all cases.

Name	LN ₂ Velocity/m·s ⁻¹	Foam Solution Velocity/m·s ⁻¹	Distance/mm	Spoiler Shape
Case 0	0.25	0.57	–	–
Case 1-1	0.25	0.57	10	Cone
Case 1-2	0.25	0.57	20	Cone
Case 1-3	0.25	0.57	30	Cone
Case 1-4	0.25	0.57	40	Cone
Case 2-1	0.25	0.57	10	Cone
Case 2-2	0.50	0.57	10	Cone
Case 2-3	0.75	0.57	10	Cone
Case 2-4	1.00	0.57	10	Cone
Case 3-0	0.50	0.57	–	–
Case 3-1	0.50	0.57	10	Cone
Case 3-2	0.50	0.57	10	Semisphere
Case 3-3	0.50	0.57	10	Spiral

2.4. Solution Methods

The mathematical models mentioned in Section 2.2 are built in ANSYS Fluent, including an RNG *k-ε* turbulent model, a mixture multiphase flow model, and an evaporation-condensation model. The evaporation of liquid nitrogen and the foaming process change with time hence the transient state is chosen. The pressure-based solver is adopted in the calculation, where the pressure is derived from the continuity equation and momentum equation to correct the velocity and satisfy the continuity [31]. The pressure-velocity coupling scheme is fixed as PISO, which is advanced in the problem that the pressure calculated by the SIMPLE algorithm deviates too much from the momentum equation [32]. In addition, the governing equations are solved by the second-order upwind method to increase the accuracy of the solution. The residual convergence criteria are specified as 1×10^{-3} for continuity, momentum, volume fraction, and turbulence equations, and 1×10^{-6} for the energy equation. The time step size of the transient state is set to 0.001 s, whose Courant number is below one in all cases to make sure our cases will never diverge.

2.5. Mesh Independence

The mesh of the foam generator combines structured meshes (hexahedrons) with unstructured meshes (tetrahedrons) in the ICEM CFD software, as shown in Figure 1. The meshes are locally densified in the area where the characteristics of flow and heat transfer are complex, such as the region near the spoiler. The number of meshes is important for the accuracy of CFD simulation results. The more meshes, the more accurate the results are [33], but they require more memory and solving time. To achieve a balance between economy and accuracy, the mesh independence (Case 1-1) is verified by four sizes, including 3.0 mm, 4.0 mm, 5.0 mm, and 6.0 mm, with 1,220,529, 494,012, 256,905, 162,642 mesh elements, respectively. A global scale factor at 3.0 mm is regarded as a criterion for verifying the calculation differences, as shown in Figure 1b. For the averaged volume fraction at various X-positions, the maximum difference between 6.0 mm and 3.0 mm is 4.48%, and the value between 5.0 mm and 3.0 mm is 3.12%, while the maximum difference between 4.0 mm and 3.0 mm is only 0.88%. To save computation time, 4 mm is selected for all simulations.

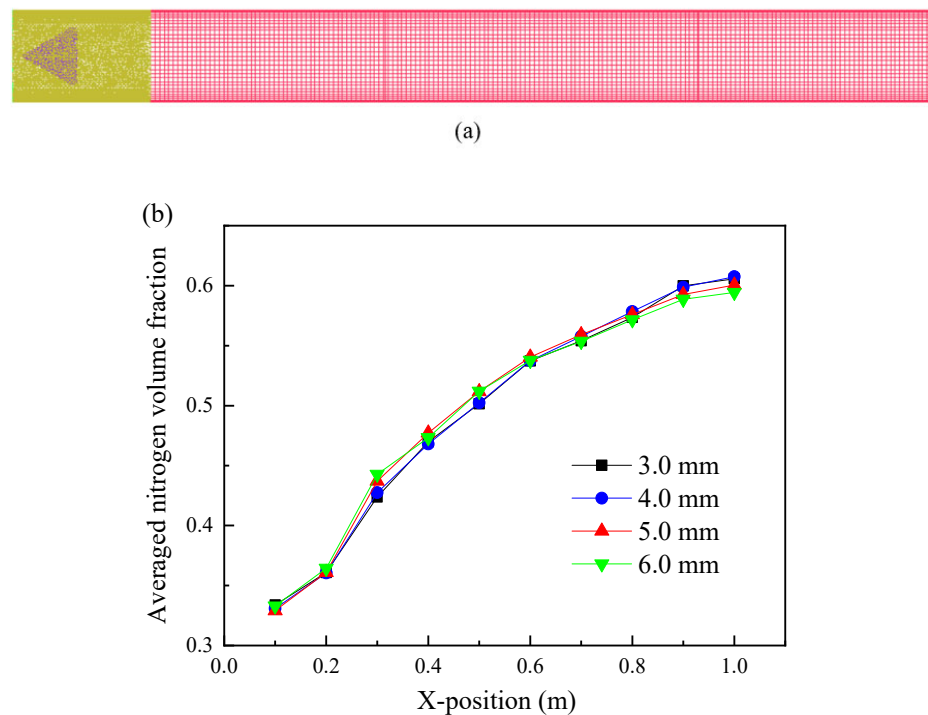


Figure 1. The schematic diagram of meshing (a) and the results of mesh independence (b).

2.6. Model Validation

Zhou et al. [21] developed a foam generator to figure out the foaming characteristics of liquid nitrogen foam in experimental and numerical methods. They compared the differences that nitrogen was mixed with water and foam solution in a foam generator, respectively. Then, they measured the temperatures that were close to the central axis (test points 6-1, 1-4, 2-4, 3-4, 4-4, and 5-4) and wall (test points 1-1, 2-1, 3-1, 4-1, and 5-1) of foam generator. They found the temperature of the nitrogen/foam solution (blue line) was higher than with nitrogen/water (black line), which indicated that the mixing efficiency of the nitrogen/foam solution was higher, due to its lower surface tension. Meanwhile, the downstream temperature was close to bulk fluid, which showed that the latent heat of evaporation worked little on the whole mixing flow.

In this work, the geometry model and boundary conditions that are similar to Zhou's experimental work are employed to validate the simulation model, and the detailed parameters of the experiment can be found in Ref. [21]. According to the results, the temperatures of test points, which were located on the central axis of the foam generator, have good agreement with their experimental data in Figure 2a, with a maximum relative deviation of less than 5.0%. As for the test points near the wall of the foam generator, the maximum relative deviation is only 1.8% compared to Zhou's work, as shown in Figure 2b. There are still some differences between our work and Zhou's work because the simulation conditions are ideal, while the RPT process of the experiment is complex and changeable. For example, the temperature difference (green line and blue line) in Figure 2b, the reason why the temperatures of simulation at the positions near the shell of the foam generator are higher than the experiment is that a constant temperature of the wall was set as 283.15 K, but the shell has heat conduction, heat convection, heat radiation, which may bring about some heat loss in experiments. Thus, the temperature (green line) in Figure 2b is relatively higher than Zhou's work (blue line). Although some parts of our simulations were ideal, these proofs can indicate that the model is suitable for the foaming process of the liquid nitrogen foam.

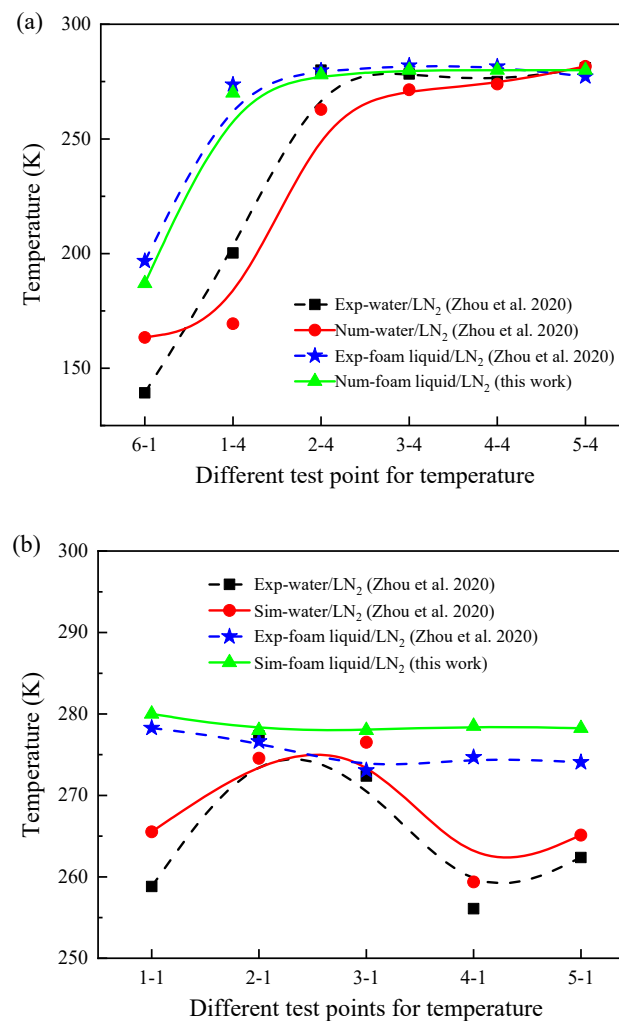


Figure 2. The results of model validation (a,b) [21].

This section may be divided by subheadings. It should provide a concise and precise description of the experimental results, their interpretation, as well as the experimental conclusions that can be drawn.

3. Results and Discussion

3.1. The Flow and Heat Transfer Characteristics of the Foaming Process

Without a spoiler, nitrogen in a foam generator is distributed at the top of the foam generator, because of the density difference between the foam solution and gas nitrogen, which indicates that its flow pattern is a stratified flow, as shown in Figure 3a. Thus, the foam solution at the bottom of the foam generator will be wasted, and the foaming process is not sufficient. In contrast to a foam generator with a cone spoiler, the liquid-liquid interface is considerably expanded. Although the stratified flow caused by density difference is inevitable, the foaming performance has been improved by the cone spoiler. The performance of the foam generator can be assessed by the volume fraction of nitrogen [21] and the uniformity of foam [34] at the end of the foam generator. If the same flow rate of foam solution and liquid nitrogen are input at the inlets, the more volume of nitrogen at the outlet, the more liquid nitrogen evaporates into nitrogen during the foaming process, where the foam may contain more nitrogen and is good for fire extinguishing. As for the uniformity of foam, some attention should be paid to the spatial distribution of nitrogen and foam solution at radial distribution, which can be shown by the contour of the volume of nitrogen at the outlet. In this work, the N₂ volume fractions at the outlet, with and without a spoiler, reach 0.529 and 0.608, respectively, and the uniformity of the nitrogen

foam at the outlet is improved by a cone spoiler as shown in Figure 3b. Another position with a high nitrogen concentration appears behind the spoiler ($x = 0.07$ m, spoiler tail), due to of the enhanced turbulence intensity. The LN₂ impinges on the cone spoiler and breaks into droplets earlier, therefore, the jet length of the LN₂ is shorter than that with no spoiler, as shown in Figure 3d. The LN₂ flow rate in Case 0 and Case 1-1 is $0.159 \text{ m}^3 \cdot \text{h}^{-1}$, and the foam solution flow rate is $15.8 \text{ m}^3 \cdot \text{h}^{-1}$. In general, these two temperature distributions are similar, due to the huge difference in flow rate between LN₂ and foam solution.

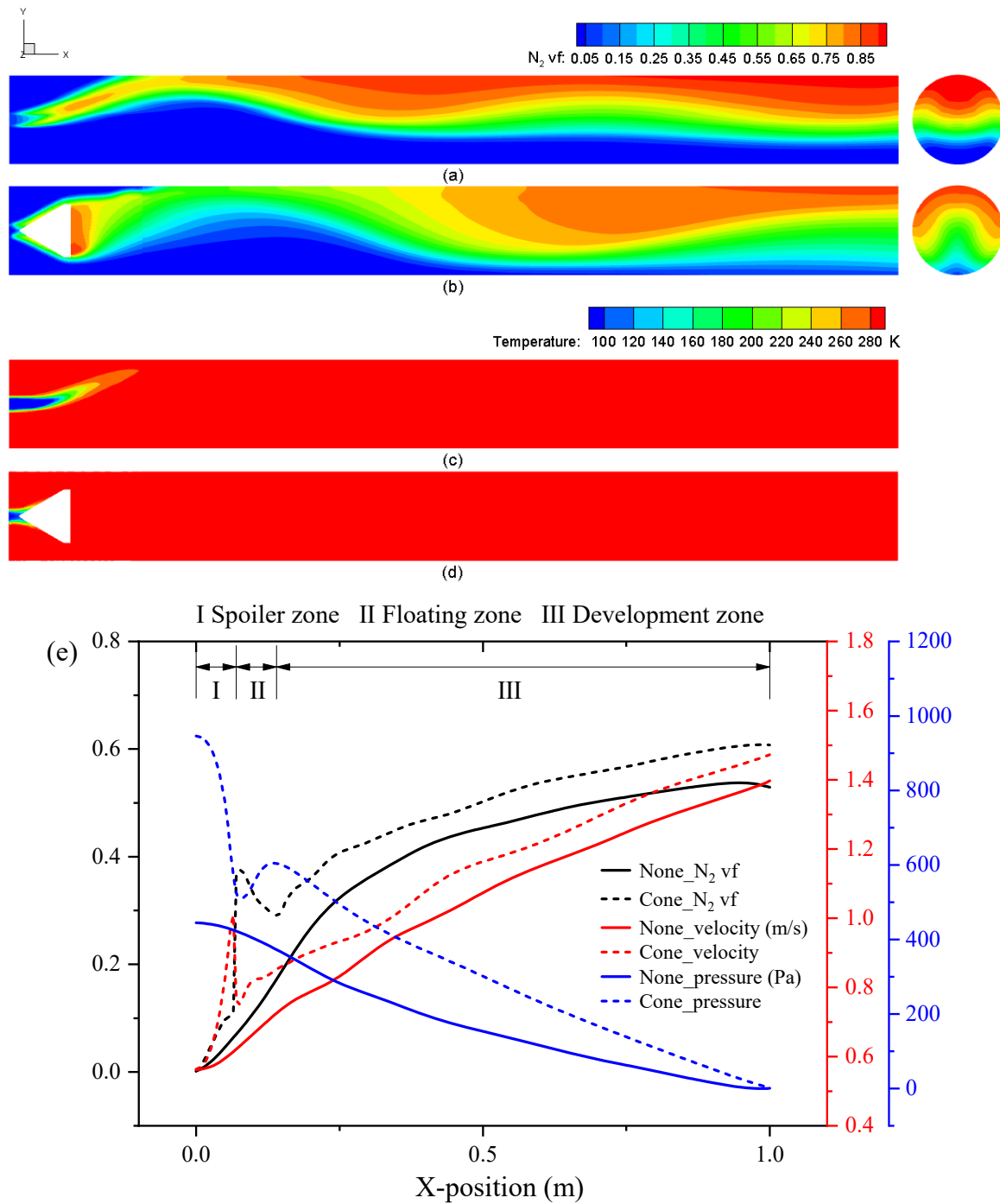


Figure 3. The N₂ volume fraction and temperature distributions of Case 0 and Case 1-1 at Z = 0 mm and outlet positions (a–d), and their quantitative distributions of N₂ volume fraction, velocity, and pressure at X-positions (e).

The quantitative analyses on averaged N_2 volume fraction, velocity, and the pressure of cross sections at X-positions, with and without a spoiler, are shown in Figure 3e. Without a cone spoiler, the static pressure is gradually converted into dynamic pressure, and the nitrogen volume fraction increases steadily to 0.529 at the outlet. If the foam generator is equipped with a cone spoiler, the foaming process can be divided into a spoiler zone, a floating zone, and a development zone. As the LN_2 runs into the cone spoiler and scatters into droplets, the N_2 volume fraction rises in the spoiler zone, compatible with the results of Ref. [21]. The cone spoiler not only narrows the flow channel to increase the velocity of the fluid, but also helps to increase the contact area between nitrogen and the foam solution. The N_2 volume fraction and velocity reach the local maximum behind the cone spoiler at $x = 0.07$ m, as well as the minimum of the pressure. Then, the foam generator is reverted to a pipe behind the spoiler. The descent section of the N_2 volume fraction appears as the foam solution at the top of the pipe flows downward due to gravity and occupies more volume, as shown in Figure 4b. Thus, it is restricted for N_2 to float up and displace the foam solution before the local minimum of the nitrogen volume fraction ($x = 0.14$ m). The nitrogen continues to accumulate in the development zone and is similar to the foaming process of a foam generator without a spoiler but performs better. The same boundary conditions of the outlet are set for two cases with a pressure of 0 Pa, leading to the comparable pressure distribution near the outlet. It can be found that the trend of N_2 volume fraction is opposite to pressure, but similar to velocity.

To further describe the flow characteristics more clearly, the nitrogen volume fraction distributions and velocity distributions at several cross sections are given in Figure 4. The black circle in Figure 4 is the projection of the cone spoiler to make clear the position of the spoiler relative to the foam generator. The first position ($x = 0.07$ m) is the distribution at the spoiler tail where the nitrogen is enriched. The foam solution begins to flow downward due to gravity, causing the velocity of the lower part of the pipe to be faster than the upper. The second position ($x = 0.14$ m) is the local minimum of the N_2 volume fraction, where a mass of nitrogen contains two high concentration nitrogen cores with a low velocity. Due to a lower density, N_2 floats up and deviates from the original position to form two symmetrical vortices, as shown in Figure 4n. The other eight positions belong to the development zone ($x > 0.14$ m), showing the coalescence and accumulation process of two nitrogen cores. The nitrogen cores rise to the top of the pipe, and the foam solution slides to the pipe bottom at $x = 0.20$ m. When the foam solution reaches the bottom, the velocity vectors on both sides are opposite, causing the formation of two symmetrical vortices at the lower part of the pipe at the third position ($x = 0.30$ m). These two opposite velocities collide with each other, thus causing the foam solution to rise briefly. Meanwhile, nitrogen is still floating toward the top and filling the vacancy provided by the foam solution. Therefore, two symmetrical vortices, whose rotation directions are opposite to the lower part, are formed in the upper part. The fifth position ($x = 0.40$ m) is where the rising foam solution falls, and the nitrogen cores continue to rise, which enhances the upper two vortices. Two nitrogen cores merge into one body, and the upper two symmetrical vortices are enhanced at $x = 0.50$ m. Even though the foam solution flows down to the bottom, their momentums dissipate with slight swings rather than disappear immediately. The foam solution still tends to rise before $x = 0.63$ m. The high concentration nitrogen accumulates on the top of the pipe and tends to squeeze the low concentration nitrogen near the pipe wall, which leads to the phenomenon that the velocity direction of the pipe center is opposite at $x = 0.63$ m. Herein, the momentum of the foam solution is completely consumed, and the solution settles at the bottom. Then the high concentration nitrogen body floats to the top of the pipe at $x = 0.70$ m and 0.80 m. At the position near the outlet ($x = 0.90$ m), the high concentration nitrogen is distributed on the top, and two vortices are formed. The nitrogen concentration reaches a certain limit and nitrogen slides downward at the pipe wall and floats up in the center of the pipe. It indicates that the distribution of nitrogen is closely bound up with its flow characteristics. The volume fraction of the nitrogen tends to be more uniform during

the foaming process by using the foam generator with a cone spoiler, which indicates that the nitrogen and foam solution also mixed more uniformly.

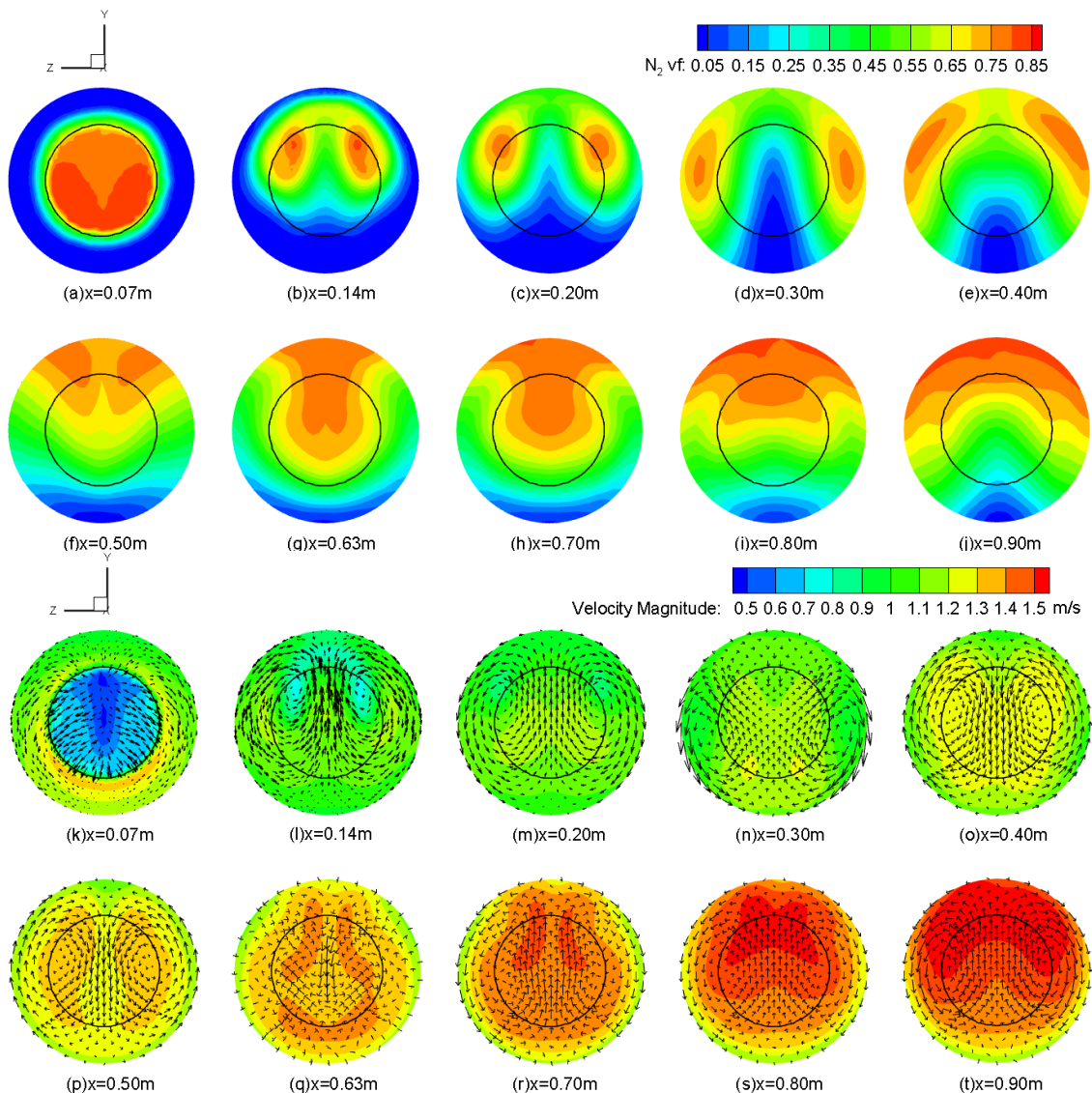


Figure 4. The distributions of the nitrogen volume fraction and velocity of ten cross sections at X-positions (Case 1-1).

3.2. Factors Affecting the Foaming Performance

3.2.1. Distance between the Inlets and Spoiler

The series of Case 1 is selected to investigate which distance is preferable for the foaming process. The correlation between the distance and nitrogen volume fraction of cross sections at X-positions is shown in Figure 5. The purpose of the spoiler is to smash the LN₂ into droplets, enhance the turbulence intensity, and form a more uniform nitrogen foam at the outlet. Regardless of the distance, the N₂ volume fraction of the foam generator with a spoiler is higher than without a spoiler. The local maximum of the N₂ volume fraction is behind the spoiler and varies with the distance. The smaller the distance, the greater the N₂ volume fractions at the spoiler tail and outlet are. In fact, the closer the distance is, the higher the growth rate of the N₂ volume fraction. If the spoiler is placed too far, it will not work effectively for breaking the liquid nitrogen into droplets; for example, when the distance exceeds 30 mm, the influence of the spoiler on the nitrogen volume fraction at the outlet is very small. Thus, the foaming performances of the foam generator with larger distances are similar to the foam generator without a spoiler, and the uniformity

of nitrogen foam will be weakened as mentioned in Section 3.1. In general, the distance of 10 mm shows better foaming performance than the other three distances.

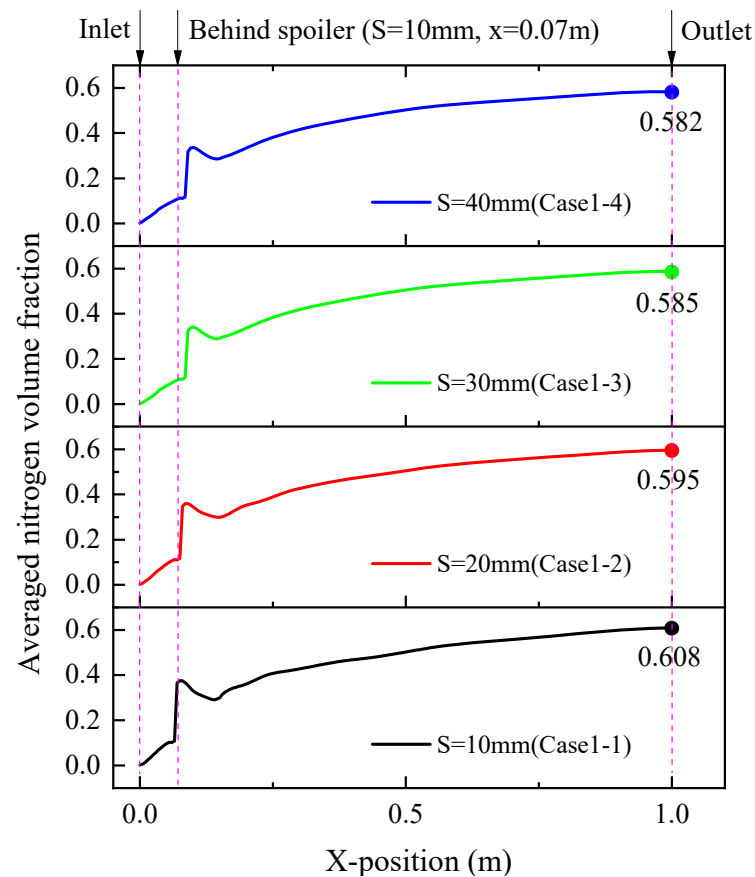


Figure 5. The N_2 volume fraction of cross sections at X-positions with different distances between inlets and cone spoiler (Case 1 series).

3.2.2. Flow Rate of the Liquid Nitrogen

The Case 2 series is chosen to select the best LN_2 flow rate using the optimal distance above. As the flow rate of the LN_2 increases proportionally, the N_2 volume fraction at the outlet changes little after reaching a certain value, which has been pointed out by Chen [35]. Meanwhile, the temperature fluctuates obviously at several key positions (e.g., Case 2-1), as shown in Figure 6. A slight peak appears near the LN_2 inlet in Case 2-1 and Case 2-2, because the flow rate of the LN_2 is too small to maintain a low temperature. The LN_2 will evaporate into N_2 around the cone spoiler, which absorbs a lot of heat and keeps the temperature down. Combined with the N_2 distribution shown in Figure 3b, the low-temperature nitrogen mainly concentrates at the spoiler tail ($x = 0.07$ m), rather than at the edge of the spoiler [21]. The average temperature rises first and then falls at the spoiler tail, due to the distribution of low-temperature nitrogen. Then the temperature difference between nitrogen and foam solution becomes smaller, and the average temperature of the cross sections gradually approaches the temperature of the bulk fluid. The change rate of the average temperature is negatively correlated with the LN_2 flow rate.

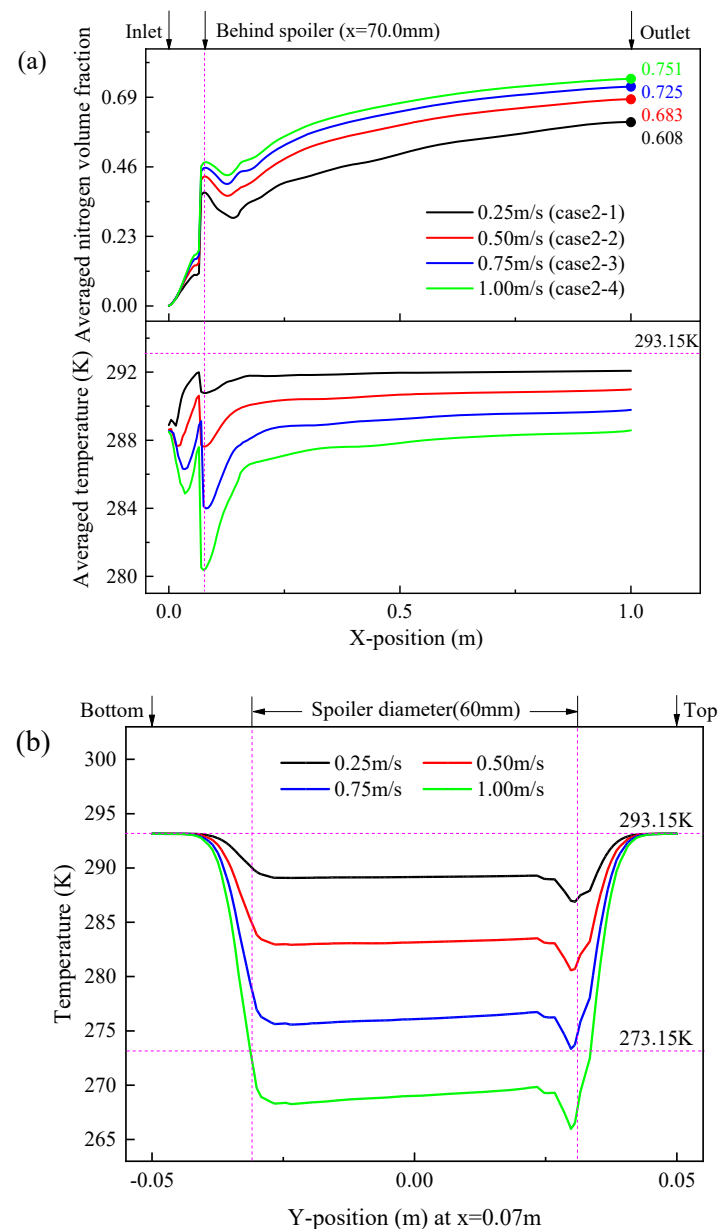


Figure 6. The N_2 volume fraction and the temperature of cross sections at X-positions (a), and the temperature of Y-positions at $x = 0.07$ m (b), with different LN_2 flow rates.

Excessive LN_2 will cause a possible phenomenon that the foam solution may freeze, corresponding to the literature [21]. Even if a large amount of LN_2 is near the inlets, it will not lead to ice formation, because the LN_2 is broken into small droplets by the cone spoiler. The minimum average temperature of the cross section is at the spoiler tail ($x = 0.07$ m), where the lowest temperature exists. The temperature in the central axis (Y-axis) of the cross section at $x = 0.07$ m is extracted as shown in Figure 6b. In accordance with the boundary conditions, the temperature of the position near the pipe wall descends from 293.15 K. The asymmetry of the curves is caused by the density and temperature differences of fluids between the upper and lower sides of the spoiler. After impacting the spoiler, the LN_2 is close to the spoiler and gasifies into N_2 , according to Figure 3b. The higher velocity at the lower side of the spoiler enhances the turbulence intensity of the multiphase fluid [21], hence the LN_2 at the lower side evaporates into nitrogen earlier than on the upper. In addition, the temperature of the LN_2 is lower than the N_2 , which explains that the lower temperature appears at the position of $y = 0.03$ m (the radius of the cone spoiler is 30 mm).

When the LN₂ velocity is 0.75 m·s⁻¹, the temperature in Figure 6b is close to 273.15 K locally, with a certain probability of ice formation. To avoid freezing in the foam generator and get a higher volume fraction of nitrogen, it is reasonable to pick the optimal velocity of the LN₂ as 0.5 m·s⁻¹, which is equal to a volume flow of 0.3 m³·h⁻¹ ($Q_{LN_2}: Q_{fs}= 1:50$).

Four cross section distributions with a flow rate of 1:50 at $x = 0.07$ m are shown in Figure 7. The cross section is adjacent to the spoiler ($x = 0.0695$ m). The lowest temperature (red curve) in Figure 6b is the position near the top vertex (0.07 m, 0.03 m, 0 m) of the black circle. The minimum temperatures of the cross section in Figure 7a, near the positions (0.07 m, 0.02 m, -0.02 m) and (0.07 m, 0.02 m, 0.02 m), are about 275 K. These two regions correspond to the position with a higher LN₂ volume fraction in Figure 7c. The reason is that the LN₂ has a hard time climbing the spoiler due to gravity [21], and the liquid nitrogen on the top of the spoiler evaporates slower than on the bottom, owing to a lower velocity than that at the bottom. Then the residual LN₂ will absorb a large amount of heat and evaporate into N₂, with the highest mass transfer rate locally in Figure 7b. Nitrogen is enriched mostly behind the spoiler, because of the local minimum pressure.

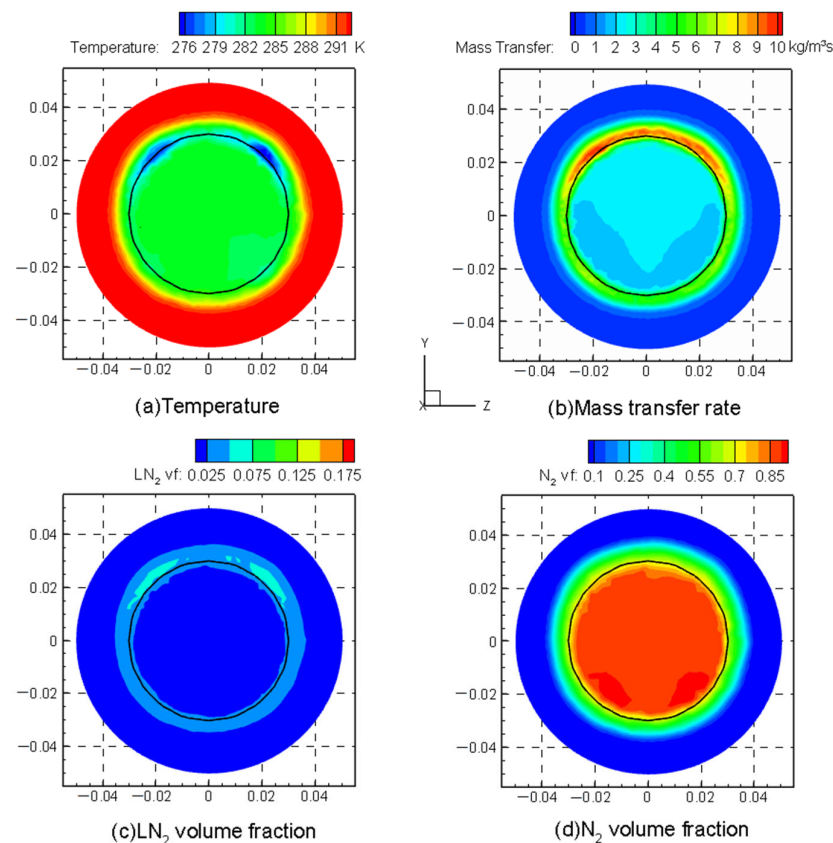


Figure 7. The distributions of the temperature (a), mass transfer rate (b), LN₂ volume fraction (c), and N₂ volume fraction (d) at $x = 0.07$ m (Case2-2).

3.2.3. Different Shapes of the Spoiler

Based on the optimal distance and LN₂ flow rate, three shapes of spoiler (Case 3 series) are simulated. The N₂ volume fraction distributions at $z = 0$ mm and outlet are shown in Figure 8. The flow pattern of the first three foam generators is a stratified flow, especially with no spoiler, which is similar to Zhou's work [21]. The flow characteristics of the foam generator with a semisphere spoiler are parallel to a cone spoiler, due to the similar shape. The foam generator with a spiral spoiler increases the turbulence intensity as a whole. Herein, the injected LN₂ impinges the cylinder spoiler, breaks into droplets, and rotates with the foam solution in the spiral channel. The N₂ and foam solution move in rotation rather than translation, which eases the stratification of multiphase fluid and promotes the

uniformity of nitrogen at the outlet. The N_2 volume fraction increases gradually, and it reaches the maximum at the outlet.

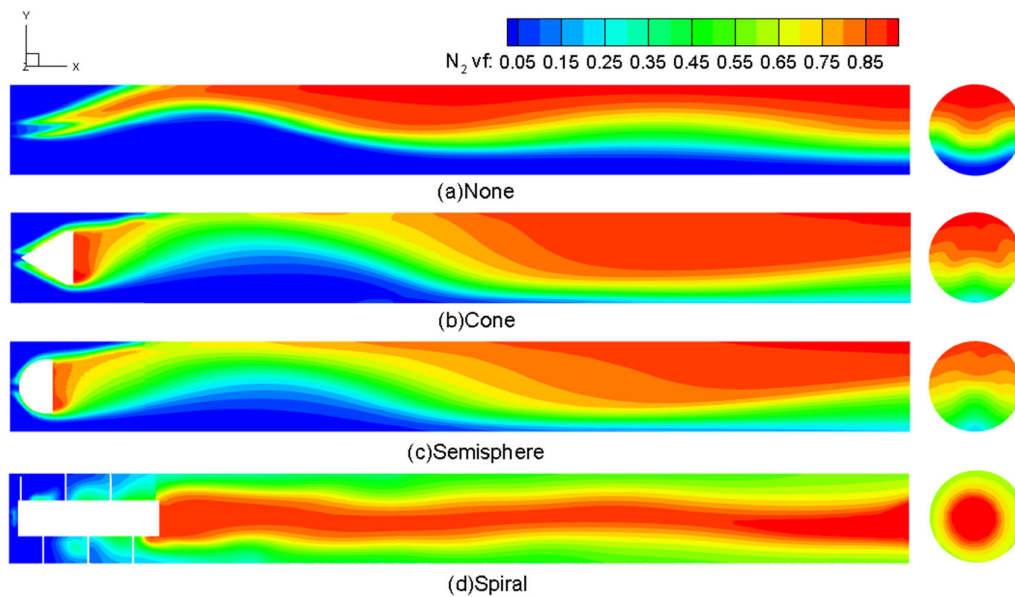


Figure 8. The nitrogen volume fraction distributions of four shaped spoilers at $z = 0$ mm and outlets (a–d).

To better understand the flow and heat transfer characteristics of the spiral spoiler, the N_2 volume fraction and velocity distributions of cross sections at five X-positions are shown in Figure 9. The LN_2 evaporates into N_2 around the cylinder spoiler, and the foam solution tends to move counterclockwise in the spiral channel. The centrifugal force has a remarkable effect on increasing the velocity near the spiral spoiler ($x < 0.09$ m). Nitrogen is concentrated directly behind the cylinder spoiler ($x = 0.16$ m) with a lower velocity, while the foam solution with a higher velocity distributes near the pipe wall. The last three positions ($x = 0.30, 0.50, 0.90$ m) demonstrate that the foam solution and the nitrogen are well mixed into a relatively homogeneous distribution over time and space. A feature can be found that the place with a larger nitrogen volume fraction also has a lower velocity.

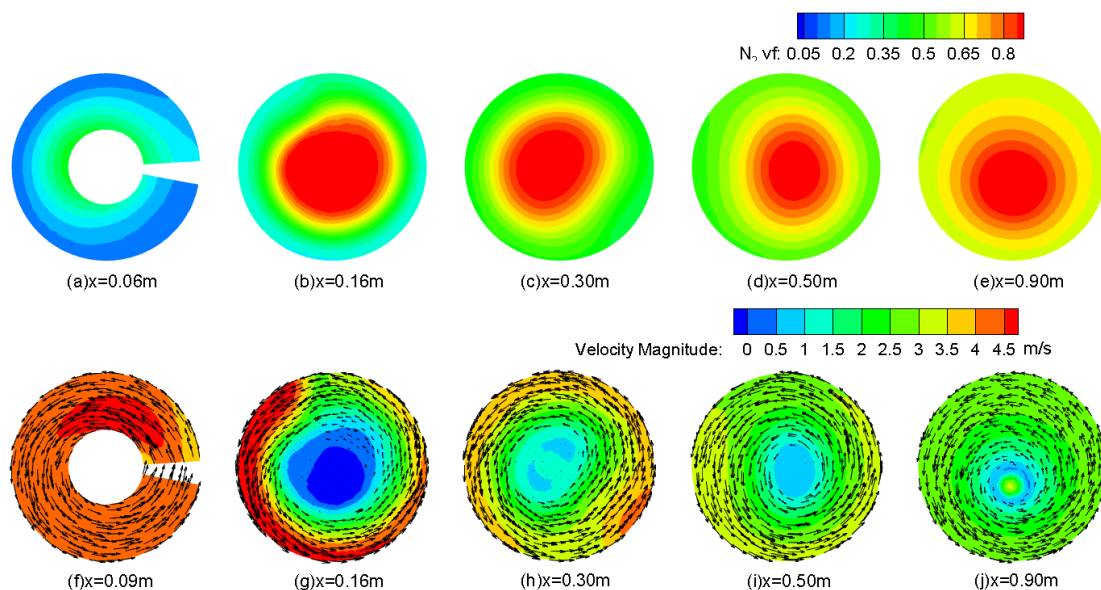


Figure 9. The N_2 volume fraction and velocity distributions of cross sections at five X-positions with the spiral spoiler (Case 3 series).

The quantitative N_2 volume fraction and pressure of cross sections at X-positions with differently shaped spoilers are obtained in Figure 10. The local maximum of the N_2 volume fraction is behind the spoiler, where the N_2 volume fraction reaches the inflection point, first rising and then falling. The cone spoiler and semisphere spoiler improve the foaming performance, but not as much as the spiral spoiler. There are three turns in the spiral spoiler, corresponding to three upward trends ($x < 0.16$ m) of the N_2 volume fraction, and the upward trends are continuously strengthened. When the multiphase fluid flows through the spiral spoiler, the N_2 volume fraction increases linearly. Compared with no spoiler, the spiral spoiler increases the N_2 volume fraction at the outlet from 0.616 to 0.717, and also improves the uniformity of nitrogen distribution at the outlet. It is effective to increase the nitrogen content of foam and the uniformity of foam, which improves the foaming performance of the foam generator.

The noteworthy points of the pressure distribution are similar to the N_2 volume fraction distribution, including the local maximum, the local minimum, and the outlet. The changing tendency of the N_2 volume fraction is opposite to the pressure. The pressure distribution of the semisphere spoiler is also in agreement with the cone spoiler, with a pressure drop of about 1000 Pa. Due to a higher turbulence intensity, there is more pressure drop in the spiral spoiler, with a value of around 21,000 Pa. Thus, the rotating process in the spiral spoiler needs to be controlled within a certain pressure loss, in case of the motion limitations in fire extinguishing, which is consistent with Ref. [10].

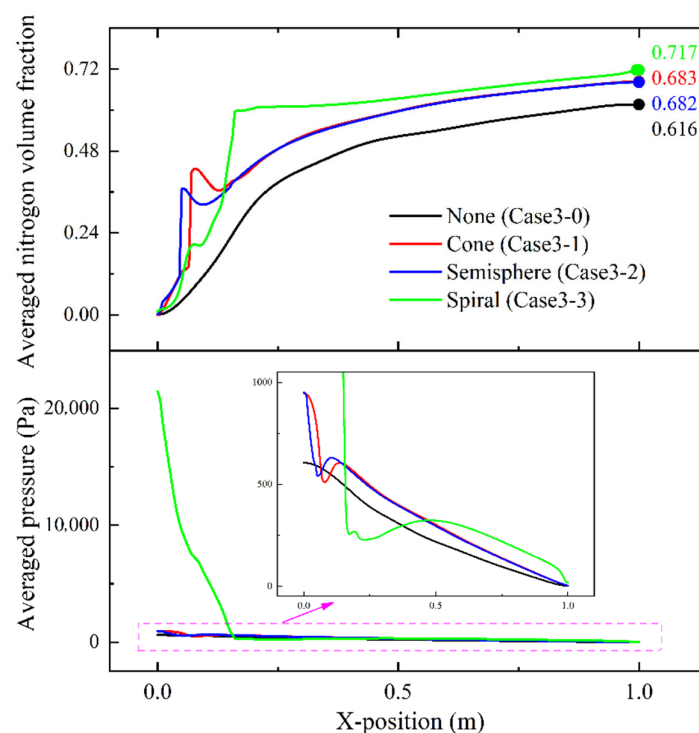


Figure 10. The N_2 volume fraction and pressure of cross sections at X-positions with different-shaped spoilers.

4. Conclusions

In this work, the flow and heat transfer characteristics of the nitrogen foam generator are investigated in numerical methods to comprehend the mechanism of its foaming process, where liquid nitrogen is used as a gas source for nitrogen. Three main factors, including the distance, LN_2 flow rate, and the shape of spoilers, are studied to provide a reference for devising a reasonable foam generator. Several conclusions can be drawn as follows:

- (1) The function of the spoiler is to smash liquid nitrogen into droplets, enhance turbulence, and improve the uniformity of foam. The foaming process of the foam generator with a cone spoiler can be divided into a spoiler zone ($x < 0.07$ m), a floating zone (0.07 m $< x < 0.14$ m), and a development zone ($x > 0.14$ m), according to the correlation between flow characteristics and nitrogen distribution.
- (2) The distance between inlets and spoiler mainly affects whether the spoiler can break liquid nitrogen into droplets. The shorter the distance, the more nitrogen is generated. Compared with the distances of 20 mm, 30 mm, and 40 mm, the optimal distance is determined as 10 mm.
- (3) With a bigger flow rate of liquid nitrogen, the volume fraction of nitrogen increases, but it may absorb more heat from the foam solution, leading to ice formation at the place with the lowest temperature (spoiler tail), which is not conducive to the fluid flow in the foaming process. Thus, a rational flow rate ratio of liquid nitrogen to foam solution is selected as 1:50.
- (4) The flow pattern of the foam generator with a semisphere spoiler is similar to that with a cone spoiler due to their similar shapes. The best shape of spoilers is the spiral, and its N_2 volume fraction at the outlet is improved from 0.616 to 0.717 compared to no spoiler, due to its circumferential motion of fluids instead of translation.

Author Contributions: Formal analysis, D.W.; Data curation, D.W.; Writing—original draft, Y.L.; Writing—review & editing, X.R.; Supervision, M.X. and H.X.; Funding acquisition, M.X. All authors have read and agreed to the published version of the manuscript.

Funding: This research received no external funding.

Data Availability Statement: Not applicable.

Conflicts of Interest: The authors declare no conflict of interest.

Nomenclature

Nomenclature

D	diameter of foam generator (mm)
L	length of foam generator (mm)
d	diameter of LN_2 inlet (mm)
S	distance between inlets and spoiler (mm)
l	generatrix length of cone spoiler (mm)
r	radius of semisphere spoiler (mm)
a	distance from blade to the front of spiral spoiler (mm)
b	blade thickness of spiral spoiler (mm)
c	length of the cylinder in spiral spoiler (mm)
W	blade height of spiral spoiler (mm)
k	turbulent kinetic energy ($m^2 \cdot s^{-2}$)
u_i	mean-velocity component in the x_i axis ($m \cdot s^{-1}$)
t	time (s)
\vec{v}_m	mass-averaged velocity ($m \cdot s^{-1}$)
n	number of phases
p	pressure (Pa)
M_m	surface tension (N)
M_k	surface tension of phase k (N)
$\vec{v}_{dr,k}$	drift velocity of phase k ($m \cdot s^{-1}$)
\vec{v}_k	velocity of secondary phase k ($m \cdot s^{-1}$)
E_k	volumetric energy of phase k ($J \cdot kg^{-1}$)
$h_{j,k}$	enthalpy of species j in phase k ($J \cdot kg^{-1}$)
$\vec{J}_{j,k}$	diffusive flux of species j in phase k ($kg \cdot m^{-2} \cdot s^{-1}$)
k_{eff}	effective conductivity ($W \cdot m^{-1} \cdot K^{-1}$)
T	equilibrium temperature of fluid (K)

k_k	conductivity of phase k ($\text{W}\cdot\text{m}^{-1}\cdot\text{K}^{-1}$)
k_t	turbulent thermal conductivity ($\text{W}\cdot\text{m}^{-1}\cdot\text{K}^{-1}$)
S_h	volumetric heat sources ($\text{W}\cdot\text{m}^{-3}$)
h_k	sensible enthalpy of phase k ($\text{J}\cdot\text{kg}^{-1}$)
\vec{v}_{pq}	relative velocity of phase p relative to phase q ($\text{m}\cdot\text{s}^{-1}$)
\vec{v}_p	velocity of phase p ($\text{m}\cdot\text{s}^{-1}$)
\vec{v}_q	velocity of phase q ($\text{m}\cdot\text{s}^{-1}$)
\dot{m}_{qp}	mass transfer from phase q to phase p ($\text{kg}\cdot\text{s}^{-1}\cdot\text{m}^{-3}$)
\dot{m}_{pq}	mass transfer from phase p to phase q ($\text{kg}\cdot\text{s}^{-1}\cdot\text{m}^{-3}$)
\dot{m}_{lv}	mass transfer by evaporation ($\text{kg}\cdot\text{s}^{-1}\cdot\text{m}^{-3}$)
\dot{m}_{vl}	mass transfer by condensation ($\text{kg}\cdot\text{s}^{-1}\cdot\text{m}^{-3}$)
$coeff$	mass transfer intensity factor (s^{-1})
T_l	temperature of liquid nitrogen (K)
T_v	temperature of gas nitrogen (K)
T_{sat}	saturation temperature of liquid nitrogen (K)
\vec{v}_v	vapor phase velocity ($\text{m}\cdot\text{s}^{-1}$)
Q_{LN2}	volume flow rate of liquid nitrogen ($\text{m}^3\cdot\text{h}^{-1}$)
Q_{fs}	volume flow rate of foam solution ($\text{m}^3\cdot\text{h}^{-1}$)
Greek symbols	
δ	thickness of the cylinder of cone and semisphere spoilers (mm)
φ	diameter of the cylinder in spiral spoiler (mm)
ε	dissipation rate
ρ	density of fluid ($\text{kg}\cdot\text{m}^{-3}$)
μ_{eff}	effective turbulent viscosity (Pa·s)
μ	dynamic viscosity (Pa·s)
μ_t	turbulent viscosity (Pa·s)
ρ_m	density of the mixture ($\text{kg}\cdot\text{m}^{-3}$)
∇	del operator
α_k	volume fraction of phase k
ρ_k	density of phase k ($\text{kg}\cdot\text{m}^{-3}$)
μ_m	viscosity of mixture (Pa·s)
α_v	vapor volume fraction
ρ_v	vapor density ($\text{kg}\cdot\text{m}^{-3}$)
α_l	liquid volume fraction
ρ_l	liquid density ($\text{kg}\cdot\text{m}^{-3}$)
Abbreviations	
N_2	nitrogen
LN_2	liquid nitrogen
CFD	computer fluid dynamics
RPT	rapid phase transition
CAFS	compressed air foam systems
AFFF	aqueous film-forming foam
CO_2	carbon dioxide
O_2	oxygen
CO	carbon monoxide
LNG	liquefied natural gas
BOG	boil-off-gas
VOF	volume of fluid
RNG	renormalization-group

References

- Reniers, G.; Cozzani, V. *Domino Effects in the Process Industries: Modelling, Prevention and Managing*; Elsevier: Amsterdam, The Netherlands, 2013; Volume 127.
- Wang, Z.-N.; Chen, J.; Cheng, W.-C.; Arulrajah, A.; Horpibulsuk, S. Investigation into the tempo-spatial distribution of recent fire hazards in China. *Nat. Hazards* **2018**, *92*, 1889–1907. [[CrossRef](#)]
- Kim, A.K.; Crampton, G.P. Evaluation of the Fire Suppression Effectiveness of Manually Applied Compressed-Air-Foam (CAF) System. *Fire Technol.* **2009**, *48*, 549–564. [[CrossRef](#)]

4. Ankit, D.; Goutham, R.; Tauseef, S.M. CFD-based study and analysis on the effectiveness of water mist in interacting pool fire suppression. *Process Saf. Environ. Prot.* **2021**, *152*, 614–629.
5. Wang, K.; Fang, J.; Shah, H.R.; Mu, S.; Lang, X.; Wang, J.; Zhang, Y. A theoretical and experimental study of extinguishing compressed air foam on an n-heptane storage tank fire with variable fuel thickness. *Process Saf. Environ. Prot.* **2020**, *138*, 117–129. [[CrossRef](#)]
6. Wang, K.; Fang, J.; Shah, H.R.; Lang, X.; Mu, S.; Zhang, Y.; Wang, J. Research on the influence of foaming gas in compressed air/nitrogen foam on extinguishing the n-heptane tank fire. *J. Loss Prev. Process Ind.* **2021**, *72*, 104533. [[CrossRef](#)]
7. Ray, S.K.; Singh, R.P. Recent Developments and Practices to Control Fire in Underground Coal Mines. *Fire Technol.* **2007**, *43*, 285–300. [[CrossRef](#)]
8. Guo, D.; Zhang, G.; Zhu, G.; Jia, B.; Zhang, P. Applicability of liquid nitrogen fire extinguishing in urban underground utility tunnel. *Case Stud. Therm. Eng.* **2020**, *21*, 100657. [[CrossRef](#)]
9. Shao, Z.; Wang, D.; Wang, Y.; Zhong, X.; Tang, X.; Hu, X. Controlling coal fires using the three-phase foam and water mist techniques in the Anjialing Open Pit Mine, China. *Nat. Hazards* **2014**, *75*, 1833–1852. [[CrossRef](#)]
10. Adamus, A. Review of the use of nitrogen in mine fires. *Min. Technol.* **2002**, *111*, 89–98. [[CrossRef](#)]
11. Zifeng, L.; Hongfang, X.; Chaoyue, Z. Liquid nitrogen gasification fracturing technology for shale gas development. *J. Petrol. Sci. Eng.* **2016**, *138*, 253–256.
12. Fu-Bao, Z.; Bo-Bo, S.; Jian-Wei, C.; Ling-Jun, M. A New Approach to Control a Serious Mine Fire with Using Liquid Nitrogen as Extinguishing Media. *Fire Technol.* **2013**, *51*, 325–334. [[CrossRef](#)]
13. Zhou, F.; Ren, W.; Wang, D.; Song, T.; Li, X.; Zhang, Y. Application of three-phase foam to fight an extraordinarily serious coal mine fire. *Int. J. Coal Geol.* **2006**, *67*, 95–100. [[CrossRef](#)]
14. Lu, X.; Wang, D.; Qin, B.; Tian, F.; Shi, G.; Dong, S. Novel approach for extinguishing large-scale coal fires using gas–liquid foams in open pit mines. *Environ. Sci. Pollut. Res.* **2015**, *22*, 18363–18371. [[CrossRef](#)]
15. Zhang, Y.; Lei, B.; Wu, B.; Meng, Y.; He, B. An Experimental Study on the Heat and Mass Transfer of Liquid Nitrogen in a Loose Medium. *Energies* **2019**, *12*, 3464. [[CrossRef](#)]
16. Aobo, L.; Michael, A.D.; Yiannis, A.L. On the trajectory and reach of fire-suppressant liquid nitrogen droplets released from a spray nozzle. *Process Saf. Environ. Prot.* **2022**, *161*, 273–284.
17. Clarke, H.; Martinez-Herasme, A.; Crookes, R.; Wen, D. Experimental study of jet structure and pressurisation upon liquid nitrogen injection into water. *Int. J. Multiph. Flow* **2010**, *36*, 940–949. [[CrossRef](#)]
18. Rupak, K.; Lokesh, R.; Arup Kumar, D. Understanding interfacial behaviour during boiling of nitrogen from liquid-liquid contact plane. *Int. J. Heat Mass Tran.* **2021**, *165*, 120661.
19. Federico, U.; Nicola, P.; Filippo, B. Loss of integrity of hydrogen technologies: A critical review. *Int. J. Hydrog. Energ.* **2020**, *45*, 23809–23840.
20. Saleem, A.; Farooq, S.; Karimi, I.A.; Banerjee, R. A CFD simulation study of boiling mechanism and BOG generation in a full-scale LNG storage tank. *Comput. Chem. Eng.* **2018**, *115*, 112–120. [[CrossRef](#)]
21. Zhou, R.; Zhang, X.; Yang, Z.; Mu, X.; Lang, X.; Wang, X.; He, L. Study on the flow characteristics of nitrogen gas foam in horizontal foam generator. *Int. J. Multiph. Flow* **2020**, *129*, 103326. [[CrossRef](#)]
22. Lu, X.; Wang, D.; Shen, W.; Wang, H.; Zhu, C.; Liu, J. Experimental investigation of the pressure gradient of a new spiral mesh foam generator. *Process Saf. Environ. Prot.* **2014**, *94*, 44–54. [[CrossRef](#)]
23. Jabarkhyl, S.; Barigou, M.; Zhu, S.; Rayment, P.; Lloyd, D.M.; Rossetti, D. Foams generated from viscous non-Newtonian shear-thinning liquids in a continuous multi rotor-stator device. *Innov. Food Sci. Emerg. Technol.* **2019**, *59*, 102231. [[CrossRef](#)]
24. Odsæter, L.; Skarsvåg, H.; Aursand, E.; Ustolin, F.; Reigstad, G.; Paltrinieri, N. Liquid Hydrogen Spills on Water—Risk and Consequences of Rapid Phase Transition. *Energies* **2021**, *14*, 4789. [[CrossRef](#)]
25. Zhongqi, Z.; Wenbing, J.; Xujin, Q.; Yonghua, H. A numerical model for liquid–vapor transition in self-pressurized cryogenic containers. *Appl. Therm. Eng.* **2021**, *193*, 117005.
26. Chen, D.; Cui, B.; Zhu, Z. Numerical simulation of the effect of upstream swirling flow on swirl meter performance. *J. Therm. Sci.* **2018**, *27*, 117–124. [[CrossRef](#)]
27. ANSYS Inc. *ANSYS Fluent Theory Guide*; ANSYS Inc.: Canonsburg, PA, USA, 2021; pp. 611–616.
28. On the Mixture Model for Multiphase Flow. Available online: <https://www.osti.gov/etdeweb/biblio/434874> (accessed on 4 March 1997).
29. Lee, W.H. *Pressure Iteration Scheme for Two-Phase Flow Modeling*; Hemisphere Publishing Corp: Scottsdale, AZ, USA, 1980.
30. Pankhurst, G.A. Foam formation and foam stability: The effect of the adsorbed layer. *Trans. Faraday Soc.* **1941**, *37*, 496–505. [[CrossRef](#)]
31. Yong, G.L. An Unstructured Grid Method for a Pressure-Based Flow and Heat Transfer Solver. *Numer. Heat Transf. Part B Fundam.* **1997**, *32*, 267–281.
32. Adam, W.; Uwe, S. Some remarks on the PISO and SIMPLE algorithms for steady turbulent flow problems. *Comput. Fluids* **1989**, *17*, 555–570.
33. Wang, L.; Zhang, Y.; Li, X.; Zhang, Y. Experimental investigation and CFD simulation of liquid-solid-solid dispersion in a stirred reactor. *Chem. Eng. Sci.* **2010**, *65*, 5559–5572. [[CrossRef](#)]

34. Xiao, J.; Chen, Z.; Shen, X.; Jiang, C.; Lu, P. Orthogonal Experiments on the Key Structural Parameters Optimization of Mine Dust Removal Foam Generator by Fluent Numerical Simulation. In Proceedings of the IOP Conference Series: Earth and Environmental Science, Anhui, China, 19 October 2018; IOP: Bristol, UK, 2019.
35. Jushi, C. Property experiments on the foam generator and its influencing factors during down-the-hole drilling. *Process Saf. Environ. Prot.* **2018**, *114*, 169–178.